

1      **Using Machine Learning Techniques for Data Quality**  
2      **Monitoring at CMS Experiment**

3      by

4      Guillermo A. Fidalgo Rodríguez

5      A thesis presented for the degree of

6      BACHELLOR'S OF SCIENCE??

7      in

8      Physics

9      UNIVERSITY OF PUERTO RICO  
10     MAYAGÜEZ CAMPUS

11     2018

12     Approved by:

13     \_\_\_\_\_  
14     Sudhir Malik, Ph.D.

15     President, Graduate Committee  
Date

16     \_\_\_\_\_  
17     Héctor Méndez, Ph.D.

18     Member, Graduate Committee  
Date

19     \_\_\_\_\_  
20     Samuel Santana Colón, Ph.D.  
21     Member, Graduate Committee

Date

22     \_\_\_\_\_  
23     Rafael A. Ramos, Ph.D.  
24     Chairperson of the Department

Date

<sup>25</sup> **Abstract**

<sup>26</sup> The Data Quality Monitoring (DQM) of CMS is a key asset to deliver high-quality  
<sup>27</sup> data for physics analysis and it is used both in the online and offline environment. The cur-  
<sup>28</sup> rent paradigm of the quality assessment is labor intensive and it is based on the scrutiny of  
<sup>29</sup> a large number of histograms by detector experts comparing them with a reference. This  
<sup>30</sup> project aims at applying recent progress in Machine Learning techniques to the automa-  
<sup>31</sup>tion of the DQM scrutiny. In particular the use of convolutional neural networks to spot  
<sup>32</sup> problems in the acquired data is presented with particular attention to semi-supervised  
<sup>33</sup> models (e.g. autoencoders) to define a classification strategy that doesn't assume previ-  
<sup>34</sup>ous knowledge of failure modes. Real data from the hadron calorimeter of CMS are used  
<sup>35</sup> to demonstrate the effectiveness of the proposed approach.

<sup>36</sup> *Keywords:* [DQM, online, offline, Machine Learning ]

<sup>37</sup> **Acknowledgments**

<sup>38</sup> I wish to thank United States State Department and University of Michigan for pro-  
<sup>39</sup> viding the opportunity to work abroad at CERN during the 2018 Winter Semester. I also  
<sup>40</sup> wish to thank CERN staff, CMS Experiment , Texas Tech University, and the University  
<sup>41</sup> of Puerto Rico at Mayagüez, with special thanks to Dr. Federico de Guio for his local  
<sup>42</sup> mentorship and Dr. Nural Akchurin, and Dr. Sudhir Malik for their guidance. A very  
<sup>43</sup> special thanks to Dr. Jean Krisch for accepting me for this great research opportunity and  
<sup>44</sup> Dr. Steven Goldfarb for being a wonderful host and overall local guidance at CERN.

# <sup>45</sup> List of Figures

46	Figure 2.1: CMS Detector . . . . .	4
47	Figure 2.2: The trajectory of a particle traveling through the layers of the	
48	detector leaving behind a it's signature footprint . . . . .	5
49	Figure 3.1: The CERN Accelerator Complex [1]. . . . .	8
50	Figure 3.2: The CMS Detector Layout [2]. . . . .	9
51	Figure 3.3: Overview of the CMS Tracker Layout [3]. . . . .	11
52	Figure 3.4: Geometrical layout of the CMS Electromagnetic Calorimeter [4].	13
53	Figure 3.5: Layout of the CMS ECAL illustrating its various components [5].	15
54	Figure 3.6: Geometrical layout of the HCAL showing the locations of the	
55	hadron barrel (HB), endcap (HE), outer (HO) and forward (HF)	
56	calorimeters [6]. . . . .	16
57	Figure 3.7: Quarter-view of the CMS muon system (left) and a muon in the	
58	transverse plane leaves a curved trajectory across the four muon	
59	detector stations (right). . . . .	18
60	Figure 3.8: Transverse slice of the CMS detector, showing the individual de-	
61	tector subsystems and particle signatures in each. The particle	
62	type can be inferred by combining the detector response in the	
63	different subdetectors [7]. . . . .	20
64	Figure 3.9: Phase-2 Pixel Detector Layout[ref]. . . . .	23

# 65 **Contents**

66	<b>Abstract</b>	i
67	<b>Acknowledgments</b>	ii
68	<b>List of Figures</b>	iii
69	<b>1 Introduction</b>	1
70	<b>2 The CMS Experiment</b>	3
71	<b>3 Data Collection and Data Quality Monitoring</b>	7
72	3.1 What is Data Collection for CMS? . . . . .	7
73	3.2 The CMS Detector . . . . .	9
74	3.2.1 Silicon Tracking System . . . . .	11
75	3.2.2 Electromagnetic Calorimeter . . . . .	13
76	3.2.3 Hadron Calorimeter . . . . .	15
77	3.2.4 Magnet . . . . .	17
78	3.2.5 Muon Detector . . . . .	17
79	3.2.6 Trigger and Data Acquisition . . . . .	19
80	3.2.7 Event Reconstruction . . . . .	20
81	3.2.8 Future Upgrade of Pixel Detector . . . . .	21
82	<b>A Appendix Title</b>	24
83	<b>B References</b>	25

<sup>84</sup> **Chapter 1**

<sup>85</sup> **Introduction**

<sup>86</sup> The work for this thesis was performed at CERN on CMS Experiment. CERN stands  
<sup>87</sup> for European Organization for Nuclear Research. It was founded in 1954 and is located  
<sup>88</sup> at the Franco-Swiss border near Geneva. At CERN, physicists and engineers are probing  
<sup>89</sup> the fundamental structure of the universe. They use the world's largest and most complex  
<sup>90</sup> scientific instruments to study the basic constituents of matter – the fundamental parti-  
<sup>91</sup> cles. The instruments used at CERN are purpose-built particle accelerators and detectors.  
<sup>92</sup> Accelerators boost beams of particles to high energies before the beams are made to col-  
<sup>93</sup> lide with each other or with stationary targets. Detectors observe and record the results  
<sup>94</sup> of these collisions. The accelerator at CERN is called the Large Hadron Collider (LHC),  
<sup>95</sup> the largest machine ever built by humans and it collides particles (protons) at close to the  
<sup>96</sup> speed of light. The process gives the physicists clues about how the particles interact, and  
<sup>97</sup> provides insights into the fundamental laws of nature. Seven experiments at the LHC use  
<sup>98</sup> detectors to analyze particles produced by proton-proton collisions. The biggest of these  
<sup>99</sup> experiments, ATLAS and CMS, use general-purpose detectors designed to study the fun-  
<sup>100</sup> damental nature of matter and fundamental forces and to look for new physics or evidence  
<sup>101</sup> of particles that are beyond the Standard Model. Having two independently designed de-  
<sup>102</sup> tectors is vital for cross-confirmation of any new discoveries made. The other two major  
<sup>103</sup> detectors ALICE and LHCb, respectively, study a state of matter that was present just  
<sup>104</sup> moments after the Big Bang and preponderance of matter than antimatter. Each experi-

105   ment does important research that is key to understanding the universe that surrounds and  
106   makes us.

107

108   [Chapter 2](#) presents a basic description of the Large Hadron Collider and CMS Detector

109

110   ?? gives a brief motivation

111

112   ?? is dedicated to a study optimizing

113

114   ?? ptimated.

115

116   ?? details an improvarger production cross-section than Z+jets process used before.

117

118   The conclusions and results of each chapter are presented in the corresponding chap-  
119   ter.

120

121   This thesis work has been presented at several internal meetings of the CMS Experi-  
122   ment and at the following international meetings and conferences:

123   1. **Andrés Abreu** gave a talk “*Estimation of the Z Invisible Background for Searches*  
124   *for Supersymmetry in the All-Hadronic Channel*” at “APS April 2018: American

125   Physical Society April Meeting 2018, 14-17 Apr 2018”, Columbus, OH

126   2. **Andrés Abreu** gave a talk “*Phase-2 Pixel upgrade simulations*” at the “USLUA

127   Annual meeting: 2017 US LHC Users Association Meeting, 1-3 Nov 2017”, Fer-  
128   milab, Batavia, IL

<sup>129</sup> **Chapter 2**

<sup>130</sup> **The CMS Experiment**

<sup>131</sup> The Compact Muon Solenoid (CMS) detector is a general purpose particle detector  
<sup>132</sup> designed to investigate various physical phenomena concerning the SM and beyond it,  
<sup>133</sup> such as Supersymmetry, Extra Dimensions and Dark Matter. As its name implies, the  
<sup>134</sup> detector is a solenoid which is constructed around a superconducting magnet capable of  
<sup>135</sup> producing a magnetic field of 3.8 T. The magnetic coil is 13m long with an inner diameter  
<sup>136</sup> of 6m, making it the largest superconducting magnet ever constructed. The CMS detector  
<sup>137</sup> itself is 21m long with a diameter of 15m and it has a weight of approximately 14,000  
<sup>138</sup> tons. The CMS experiment is one of the largest scientific collaborations in the history  
<sup>139</sup> of mankind with over 4,000 participants from 42 countries and 182 institutions. CMS is  
<sup>140</sup> located at one of these points and it essentially acts as a giant super highspeed camera  
<sup>141</sup> that makes 3D images of the collisions that are produced at a rate of 40 MHz (40 million  
<sup>142</sup> times per second). The detector has an onion-like structure to capture all the particles that  
<sup>143</sup> are produced in these high energy collisions most of them being unstable and decaying  
<sup>144</sup> further to stable particles that are detected. CMS detector was designed with the following  
<sup>145</sup> features (as shown in [Figure 3.2](#)) :

- <sup>146</sup> 1. A **magnet** with large bending power and high performance muon detector for good  
<sup>147</sup> muon identification and momentum resolution over a wide range of momenta and  
<sup>148</sup> angles.

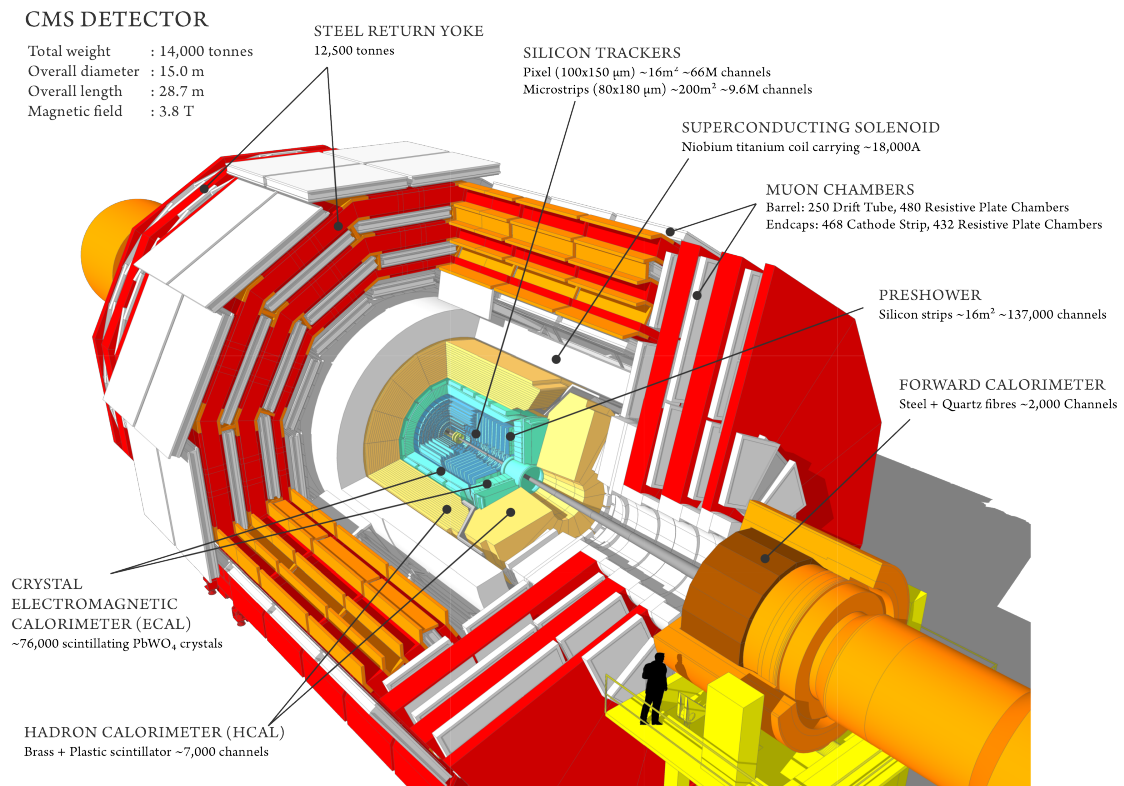


**Figure 2.1:** CMS Detector

- 149     2. An **inner tracking system** capable of high reconstruction efficiency and momen-  
150       tum resolution requiring **pixel detectors** close to the interaction region.
- 151     3. An **electromagnetic calorimeter** able to provide good electromagnetic energy res-  
152       olution and a high isolation efficiency for photons and leptons.
- 153     4. A **hadron calorimeter** capable of providing precise missing-transverse-energy and  
154       dijet-mass resolution.

155       A property from these particles that is exploited is their charge. Normally, particles  
156       produced in collisions travel in a straight line, but in the presence of a magnetic field,  
157       their paths are skewed and curved. Except the muon system, the rest of the subdetectors  
158       lie inside a 3.8 Tesla magnetic field . Due to the magnetic field the trajectory of charged  
159       particle produced in the collisions gets curved (as shown in [Figure 2.2](#) ) and one can  
160       calculate the particle's momentum and know the type of charge on the particle. The  
161       Tracking devices are responsible for drawing the trajectory of the particles by using a  
162       computer program that reconstructs the path by using electrical signals that are left by

the particle as they move. The Calorimeters measure the energy of particles that pass through them by absorbing their energy with the intent of stopping them. The particle identification detectors work by detecting radiation emitted by charged particles and using this information they can measure the speed, momentum, and mass of a particle. After the information is put together to make the “snapshot” of the collision one looks for results that do not fit the current theories or models in order to look for new physics.

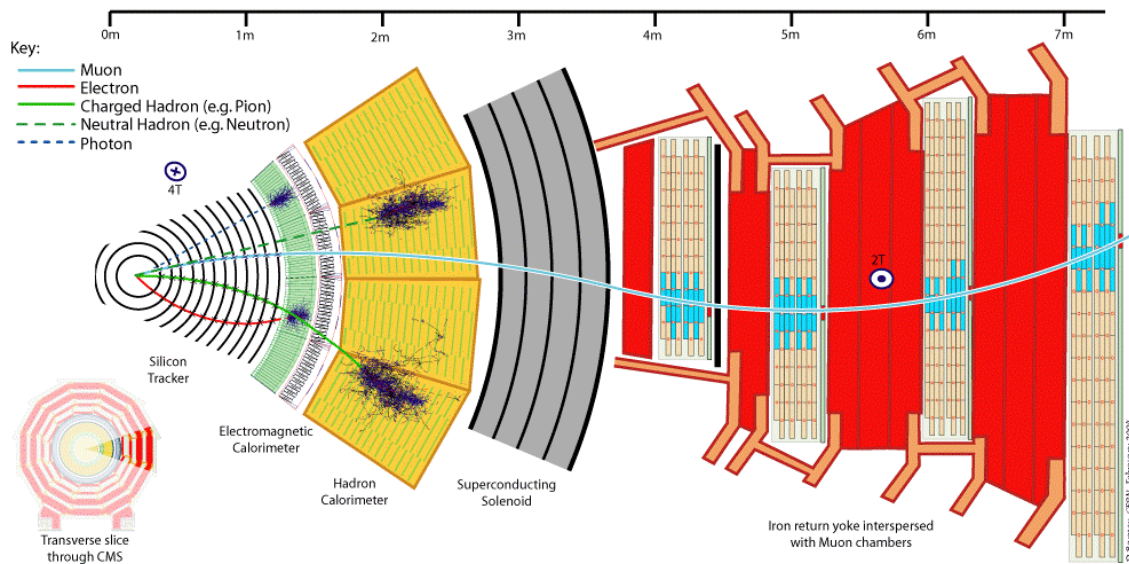


**Figure 2.2:** The trajectory of a particle traveling through the layers of the detector leaving behind a it's signature footprint

The project focusses specifically on data collected from one of the Calorimeters, - the Hadron Calorimeter (HCAL). The HCAL, as its name indicates, is designed to detect and measure the energy of hadrons or, particles that are composed of quarks and gluons, like protons and neutrons. Additionally, it provides an indirect measurement of the presence of non-interacting, uncharged particles such as neutrinos (missing energy) . Measuring these particles is important as they can tell us if new particles such as the Higgs boson or supersymmetric particles (much heavier versions of the standard particles we know) have been formed. The layers of the HCAL are structured in a staggered fashion to prevent any gaps that a particle might pass through undetected. There are two main parts: the barrel and the end caps. There are 36 barrel wedges that form the last layer of the detector inside the magnet coil, there is another layer outside this, and on the endcaps, there are another 36 wedges to detect particles that come out at shallow angles with respect to the beam

181 line.

# <sup>182</sup> Chapter 3

## <sup>183</sup> Data Collection and Data Quality

### <sup>184</sup> Monitoring

#### <sup>185</sup> 3.1 What is Data Collection for CMS?

<sup>186</sup> During data taking there are millions of collisions occurring in the center of the detector every second. The data per event is around one million bytes (1 MB), that is produced at a rate of about 600 million events per second (CERN, 2018), that's about 600 MB/s. <sup>187</sup> Keeping in mind that only certain events are considered “interesting” for analysis, the task of deciding what events to consider out of all the data collected is a two-stage process. First, the events are filtered down to 100 thousand events per second for digital reconstruction and then more specialized algorithms filter the data even more to around <sup>191</sup> 100 200 events per second that are found interesting. For CMS there is a Data Acquisition System that records the raw data to what's called a High-Level Trigger farm which is a room full of servers that are dedicated to processing and classify this raw data quickly. <sup>194</sup> The data then gets sent to what's known as the Tier-0 farm where the full processing and <sup>195</sup> the first reconstruction of the data are done. [8]

<sup>198</sup> The four main detectors comprising the LHC machine are CMS, ATLAS [9], LHCb <sup>199</sup> [10] and ALICE [11]. Both CMS and ATLAS are general purpose detectors whose initial <sup>200</sup> designs had the detection of the SM Higgs boson, with its wide range of decay modes,

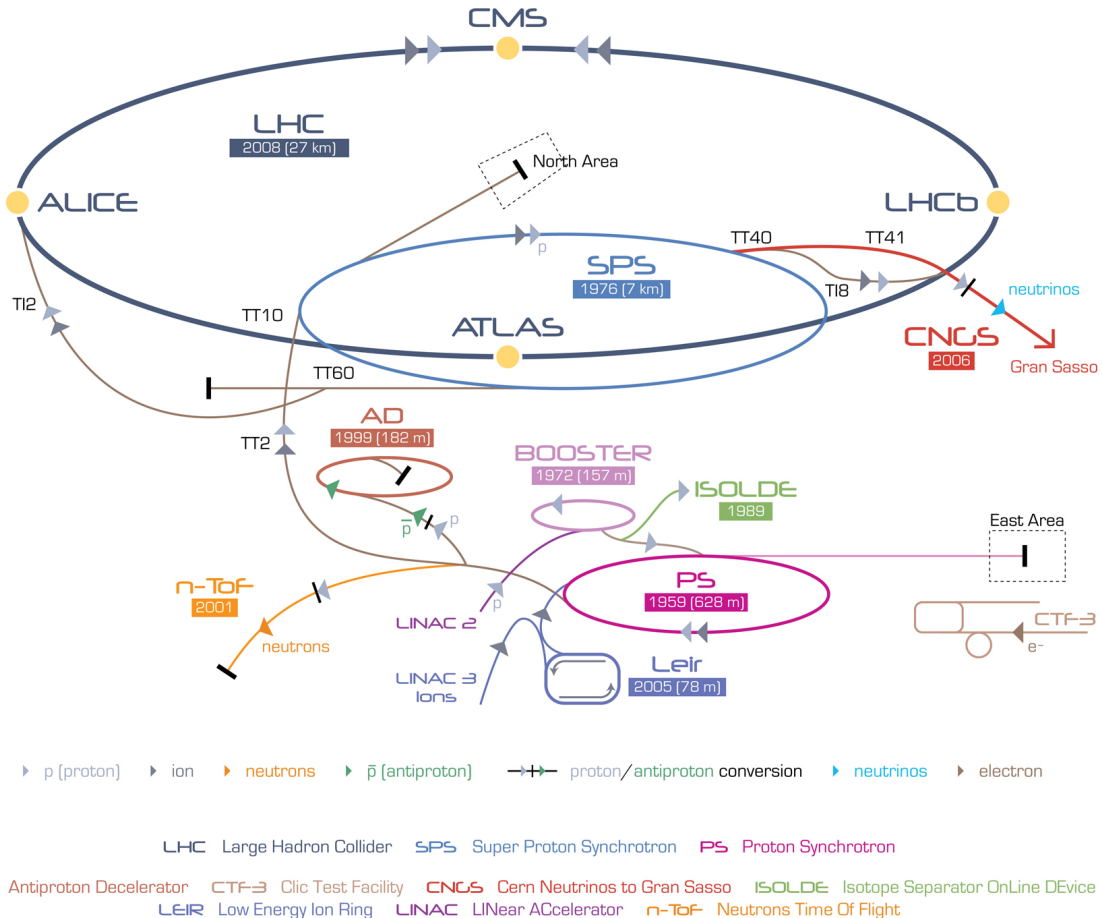


**Figure 3.1:** The CERN Accelerator Complex [1].

in mind. Both detectors managed to accomplish this goal when a 126 GeV scalar boson consistent with the SM Higgs was independently verified by both experiments in July of 2012. Furthermore, the designs for CMS and ATLAS allow for the search of many other additional phenomena in BSM physics such as Supersymmetry, Dark Matter [12], Dark Sector [13], etc. On the other hand, the LHCb and ALICE detectors focus on more particular kinds of searches. The main motivation for the LHCb experiment, where the b stands for beauty, concerns itself with the measurement of CP violation parameters in b-hadron interactions and studies cover a wide range of aspects of Heavy Flavor Electroweak and QCD physics. Meanwhile, the ALICE experiment focuses on the study of heavy ion (Pb-Pb) nuclei collisions at a centre-of-mass energy of 2.76 TeV in order to better understand the physics behind strongly interacting matter at extreme energy densities.

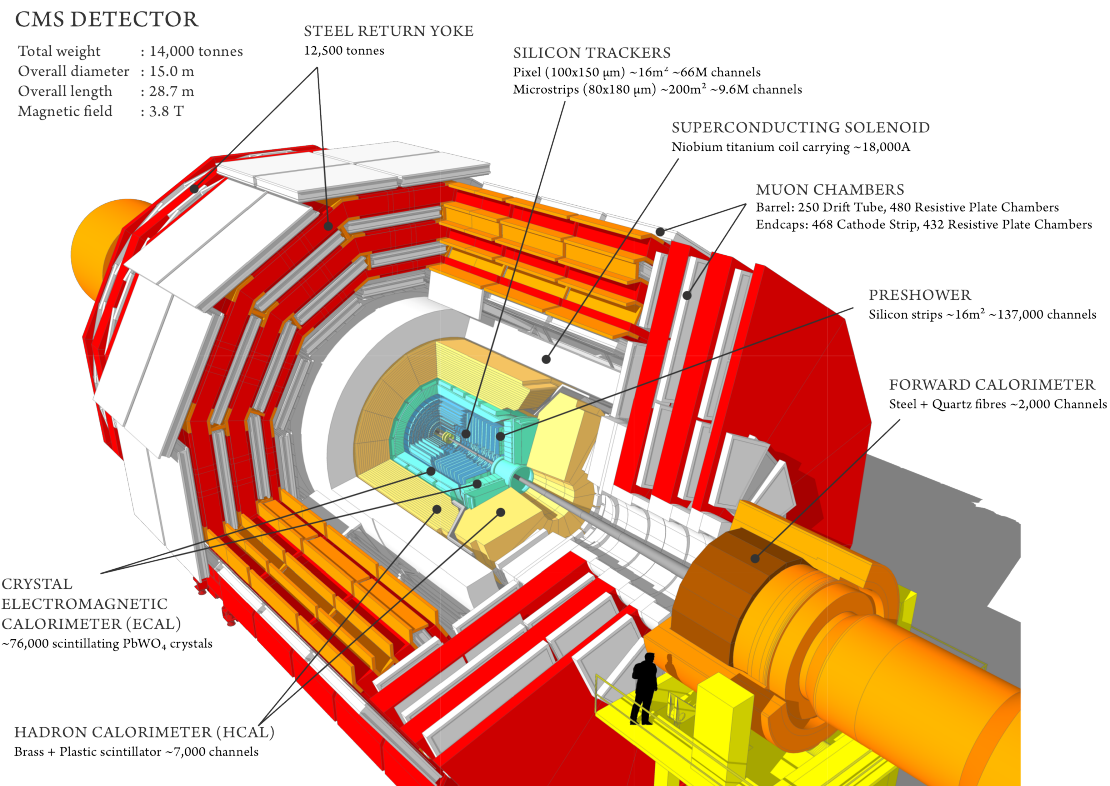


**Figure 3.2:** The CMS Detector Layout [2].

## 212    3.2 The CMS Detector

213    The Compact Muon Solenoid (CMS) detector is a general purpose particle detector  
 214    designed to investigate various physical phenomena concerning the SM and beyond it,  
 215    such as Supersymmetry, Extra Dimensions and Dark Matter. As its name implies, the  
 216    detector is a solenoid which is constructed around a superconducting magnet capable of  
 217    producing a magnetic field of 3.8 T. The magnetic coil is 13m long with an inner diameter  
 218    of 6m, making it the largest superconducting magnet ever constructed. The CMS detector  
 219    itself is 21m long with a diameter of 15m and it has a weight of approximately 14,000  
 220    tonnes. The CMS experiment is one of the largest scientific collaborations in the history  
 221    of mankind with over 4,000 participants from 42 countries and 182 institutions.

222

223    In order to meet the many needs of the SM and BSM searches, and the goals of the  
 224    LHC physics program, the CMS detector was designed with the following features:

225

- 226     • A magnet with large bending power and high performance muon detector for good  
 227       muon identification and momentum resolution over a wide range of momenta and  
 228       angles.

229

- 230     • An inner tracking system capable of high reconstruction efficiency and momentum  
 231       resolution requiring pixel detectors close to the interaction region.

232

- 233     • An electromagnetic calorimeter able to provide good electromagnetic energy reso-  
 234       lution and a high isolation efficiency for photons and leptons.

235

- 236     • A hadron calorimeter capable of providing precise missing-transverse-energy ( $p_T^{miss}$ )  
 237       and dijet-mass resolution.

238

239       A general layout of the CMS detector and all its constituent sub-detectors can be seen  
 240       in [Figure 3.2](#). The configuration of the CMS sub-detectors follow a cylindrical layer  
 241       pattern that is symmetrical about the interaction region and consists of a central barrel  
 242       with endcaps on both ends.

243       The coordinate system for the CMS detector design uses a right-hand rule conven-  
 244       tion centered around the ideal interaction point to describe the positions of objects in the  
 245       experiment. The z-axis is defined along the direction of the LHC beam, with the x-axis  
 246       pointing towards the center of the LHC ring. In terms of polar coordinates then, r is the  
 247       radial distance from the center of the pipe, the polar angle  $\theta$  is measured against the z-axis  
 248       and the azimuthal angle  $\phi$  is measured with respect to the x-axis. However, the pseudo-  
 249       rapidity  $\eta$  is generally preferred over the polar angle  $\theta$ . The pseudorapidity is defined  
 250       as:

251

$$\eta = -\ln \tan \frac{\theta}{2}.$$

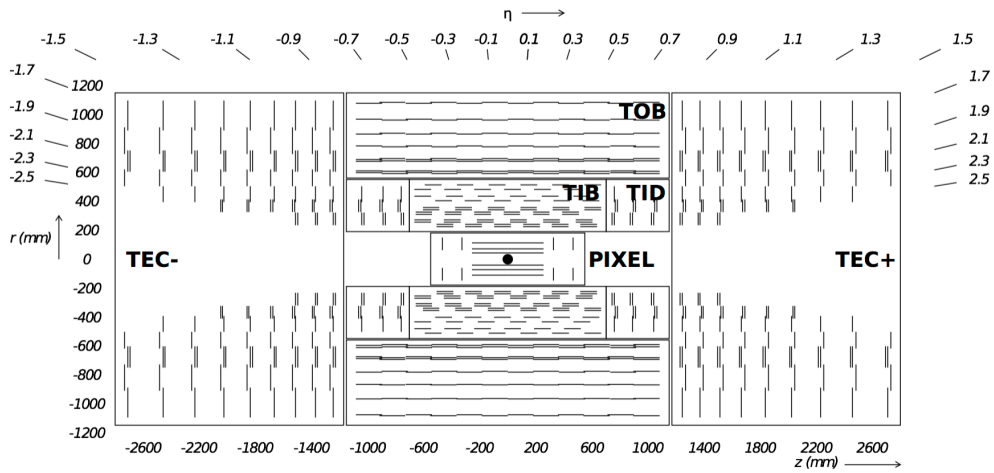


**Figure 3.3:** Overview of the CMS Tracker Layout [3].

### 252 3.2.1 Silicon Tracking System

253 The CMS tracking system was designed with the goal of obtaining precise and effi-  
 254 cient measurements for the trajectories of charged particles resulting from proton-proton  
 255 collisions at the LHC. In addition, it allows for the precise measurement of secondary ver-  
 256 tices and impact parameters needed to efficiently identify the heavy flavours produced in  
 257 many interesting physics channels. Due to the LHC's design Luminosity of  $10^{34} \text{ cm}^{-2}\text{s}^{-1}$ ,  
 258 the currently installed CMS phase-1 tracker is expected to handle an average of 1000 par-  
 259 ticles from over 20 overlapping proton-proton interactions per bunch crossing, every 25  
 260 ns. This required a detector technology capable of achieving a high granularity and fast  
 261 response as well as being tolerant to the radiation produced from the intense particle flux.  
 262 These considerations lead to a tracker design composed entirely of silicon detector tech-  
 263 nology which features an active silicon area of about  $200 \text{ m}^2$ , making it the largest silicon  
 264 tracker ever built [5].

265

266 The CMS tracker is built in a cylindrical manner around the interaction point and has  
 267 a diameter of 2.5 m and a length of 5.8 m. It is comprised of a pixel detector with three  
 268 barrel layers, positioned at a distance between 4.4 cm and 10.2 cm from the interaction  
 269 region, and a silicon strip tracker with 10 barrel detection layers extending to a radius of

270 1.1 m. Each system is made complete by endcaps at opposite sides of the barrel, consisting  
 271 of 2 discs for the pixel detector and 3 plus 9 discs for the strip tracker, extending the  
 272 acceptance region of the tracker up to a pseudorapidity  $|\eta| < 2.5$ .

273

274 The pixel detector is the part of the CMS tracking system closest to the interaction  
 275 region and consists of 3 barrel layers (BPix) and 2 endcap discs (FPix). It is responsible  
 276 for providing precise tracking points in  $r\phi$  and  $z$ , a feature that is required for the small  
 277 impact parameter resolution, needed for good secondary vertex reconstruction. The de-  
 278 tector contains 1440 modules covering an area of approximately 1 m<sup>2</sup> making up a total  
 279 of 66 million pixels. The sensors were designed using an n-on-n concept from 320  $\mu\text{m}$   
 280 thick silicon wafers and are fabricated with read-out chips (ROCs) that are bump-bonded  
 281 to the sensor in standard 0.25  $\mu\text{m}$  CMOS technology. Each of the pixels has a pitch size  
 282 of  $100 \times 150 \mu\text{m}^2$ , which corresponds to an occupancy of about  $10^{-4}$  per bunch crossing.

283

284 The silicon strip tracker is built surrounding the pixel detector and consists of three  
 285 large subsystems. The Tracker Inner Barrel and Disks (TIB/TID) extend to a radius of  
 286 55 cm and are composed of four barrel layers, completed by three disks at each end. The  
 287 TIB/TID employs the use of 320  $\mu\text{m}$  thick silicon micro-strip sensors in order to deliver  
 288 up to 4  $r\phi$  measurements on a trajectory. Surrounding the TIB/TID is the Tracker Outer  
 289 Barrel (TOB), which consists of 6 barrel layers and has an outer radius of 116 cm. The  
 290 TOB extends symmetrically in  $z$  between  $\pm 118$  cm and provides an additional 6  $r\phi$   
 291 measurements for a trajectory. Beyond the TOB's  $z$  range lie the Tracker Endcaps (TEC+  
 292 and TEC-, where the sign indicates their position respect to  $z$ ). Each TEC consists of 9  
 293 discs with up to 7 rings of silicon micro-strip detectors, providing up to 9 additional  $\phi$   
 294 measurements per trajectory. The CMS silicon strip tracker has a total active silicon area  
 295 of 198 m<sup>2</sup> and is composed of 15,148 sensor modules.

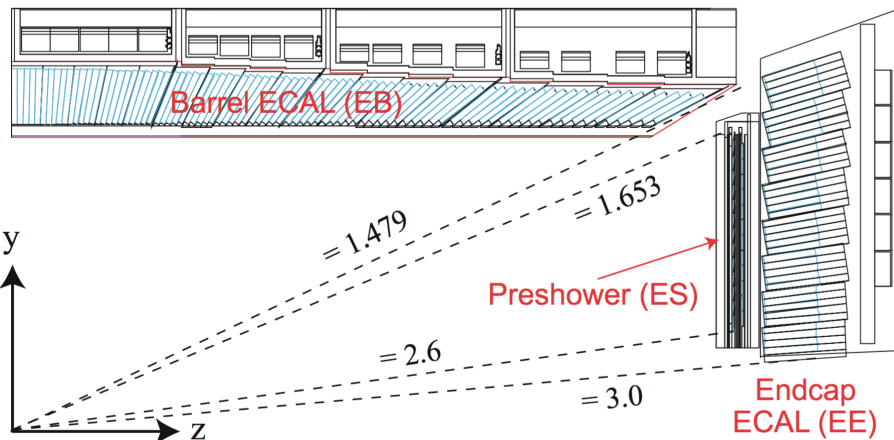


**Figure 3.4:** Geometrical layout of the CMS Electromagnetic Calorimeter [4].

### 296 3.2.2 Electromagnetic Calorimeter

297 The CMS Electromagnetic Calorimeter (ECAL) is a hermetic homogeneous calorime-  
 298 ter whose function is to measure the energy of particles that interact via the electromag-  
 299 netic force. With the use of 75,848 scintillator crystals, it is capable of providing good  
 300 energy resolution within the requirements of the ambitious LHC program. In particular,  
 301 the ECAL's design was optimized to search for diphoton events resulting from Higgs bo-  
 302 son decays ( $H \rightarrow \gamma\gamma$ ).

303

304 The ECAL is composed of two main sub-systems – the barrel calorimeter (EB) and the  
 305 endcap calorimeter (EE) – and is completed by a preshower calorimeter (ES), as shown  
 306 in [Figure 3.5](#). It covers a solid angle up to a pseudorapidity of  $|\eta| < 3$ , with the EB ex-  
 307 tending in the range of  $|\eta| < 1.479$  and the EE covering a range of  $1.479 < |\eta| < 3$ . Both  
 308 subsystems are composed of lead tungstate ( $\text{PbWO}_4$ ) scintillator crystals which provide  
 309 a fast response time and high radiation tolerance, both crucial requirements for optimal  
 310 performance at LHC operating conditions. In addition, the properties of the  $\text{PbWO}_4$  crys-  
 311 tals (high density, short radiation length and small Molière radius) led to the design of a compact  
 312 calorimeter with fine granularity.

313

314 The barrel part of the ECAL (EB) is composed of specially designed avalanche pho-

315    todiodes (APD). It consists of 61,200 crystals, forming a total volume of  $8.14 \text{ m}^3$  and  
 316    weighing about 67.4 t. The crystals that form the EB are 230 mm long with a cross-  
 317    section of  $22 \times 22 \text{ mm}^2$  at the front face and  $26 \times 26 \text{ mm}^2$  at the back. They are organized  
 318    in pairs within thin-walled alveolar structures called submodules. The submodules are  
 319    assembled into different types of modules that differ by their location with respect to  $\eta$   
 320    and contain 400 or 500 crystals each. These modules are then arranged in sets of four  
 321    modules, called supermodules, and contain 1700 crystals each. Thus, the EB is composed  
 322    of two half-barrels, each consisting of 18 supermodules.

323

324    In contrast, the photodetectors used in the endcap section of the ECAL are vacuum  
 325    phototriodes (VPT) [14]. Each of the endcaps contain 7,324 crystals which, in total, oc-  
 326    cupy a volume of  $2.90 \text{ m}^3$  and weigh about 24.0 t. The crystals in the EE are 220 mm in  
 327    length with a cross-section of  $28.62 \times 28.62 \text{ mm}^2$  for the front face and  $30 \times 30 \text{ mm}^2$  in the  
 328    rear. They are all identical in shape and are arranged in mechanical units of  $5 \times 5$  crystals,  
 329    called supercrystals (SC), which consist of carbon-fibre alveola structures. Each of the  
 330    endcaps are divided into two semi-circular structures, called *Dees*, which hold a total of  
 331    3,662 crystals.

332

333    The ES preshower is located before the EE detector and spans a pseudorapidity range  
 334    of  $1.653 < |\eta| < 2.6$ . Its main purpose is to identify neutral pions in the endcaps as  
 335    well as to improve the determination of electrons and photons with high granularity. The  
 336    preshower consists of two layers and has a total thickness of 20 cm. The first layer is  
 337    conformed by lead radiators which initiate electromagnetic showers from incoming pho-  
 338    tons and electrons. Meanwhile, the second layer is composed of silicon strips which are  
 339    capable of measuring the deposited energy and the transverse shower profiles.

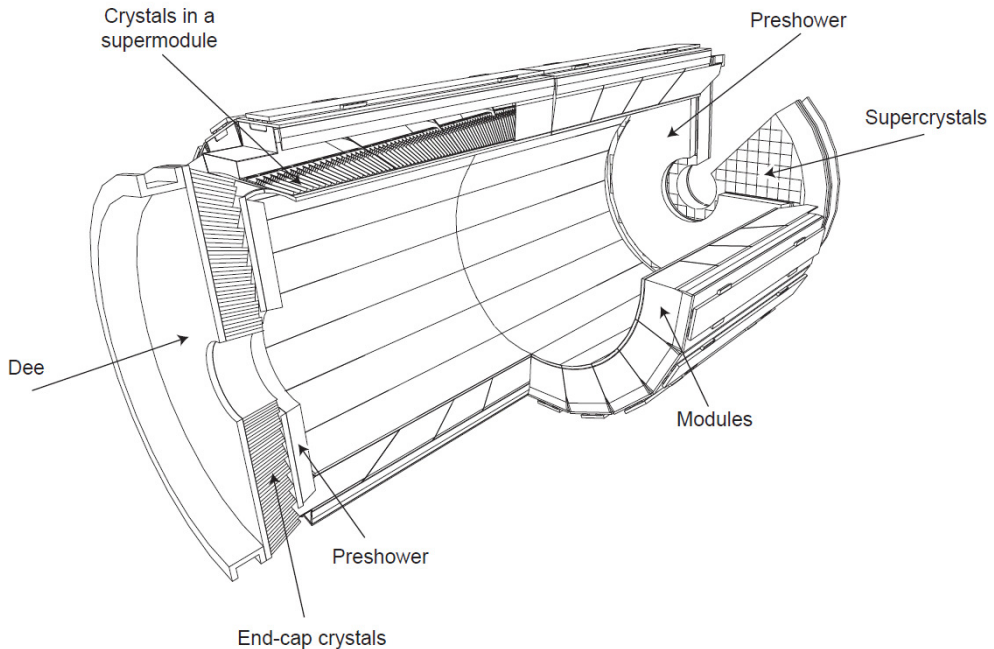


**Figure 3.5:** Layout of the CMS ECAL illustrating its various components [5].

### 3.2.3 Hadron Calorimeter

The CMS Hadron calorimeter (HCAL) conforms the next layer of the CMS detector. It is a sampling calorimeter that consists of alternating layers of massive absorbing brass plates and plastic scintillator tiles and is of particular importance for the measurement of hadron jet energy and  $p_T^{miss}$ . The HCAL detector is located in between the outer extent of the ECAL ( $R = 1.77$  m) and the inner extent of the magnet coil ( $R = 2.95$  m). Similar to the other CMS subsystems, it's composed of a barrel part (HB) and an endcap part (HE). In addition, it features a tail-catching outer calorimeter (HO), located outside the magnet, and a forward calorimeter (HF) in the very forward region near the beam line. A layout of the HCAL system can be seen in Figure 3.6.

350

The barrel component of the HCAL is a sampling calorimeter which covers the pseudorapidity range  $|\eta| < 1.3$ . It consists of both the HB and the HO detectors. The reason behind separating the barrel detector into the HB and HO is due to the limited amount of space available for the barrel detector. The HB is located within the superconducting magnet coil and is supplemented by the HO in between the outer solenoid coil and the

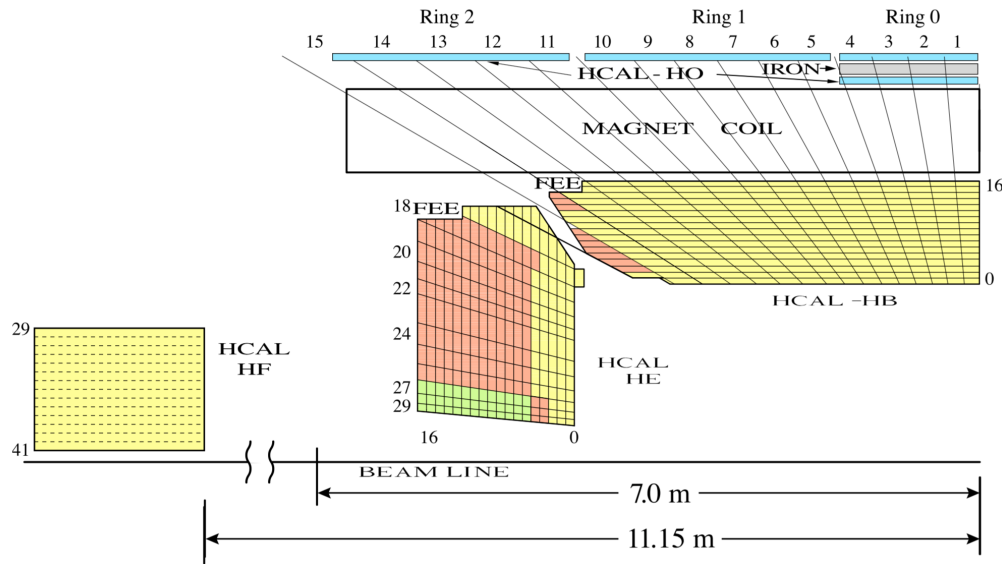


**Figure 3.6:** Geometrical layout of the HCAL showing the locations of the hadron barrel (HB), endcap (HE), outer (HO) and forward (HF) calorimeters [6].

356 muon chambers. Therefore, the HO acts as a tail-catcher in order to improve the jet en-  
 357 ergy measurements and  $p_T^{miss}$ , with the solenoid in between acting as absorber material.  
 358 The HB consists of two half-barrel sections, identified as HB+ and HB- due to their ge-  
 359 ometrical location, which are composed of 36 identical azimuthal wedges. The wedges,  
 360 which are constructed out of flat brass absorber plates, are aligned parallel to the beam  
 361 axis and are segmented into four azimuthal angle ( $\phi$ ) sections.

362

363 The HE covers a significant amount of the pseudorapidity in the range of  $1.3 < |\eta| <$   
 364 3, a region containing about 34% of the particles produced in the final state. Due to  
 365 the high luminosity of the LHC, the HE is required to have a high radiation tolerance at  
 366  $|\eta| \simeq 3$ , as well as being capable of handling high counting rates. Similar to the HB, the  
 367 HE is also composed of brass absorber plates and scintillator plates which are read out  
 368 by wavelength shifting fibers. The light captured by the scintillators merges within the  
 369 wavelength shifting fibers and then it's read out by hybrid photo-diodes. The scintillators  
 370 are partitioned in towers with an area of  $\Delta\eta \times \Delta\phi = 0.17 \times 0.17$ .

371

372 **3.2.4 Magnet**

373 The CMS superconducting solenoid is one of the driving features of the detector de-  
374 sign. It is capable of providing a magnetic field with a 3.8T magnitude, which allows  
375 for the large bending power needed for precise particle transverse momentum ( $p_T$ ) mea-  
376 surements. The magnet is made of four layers of stabilized reinforced Niobium-Titanium  
377 (NbTi) and has a cold mass of 220 t. The solenoid consists of a 13 m long coil with an  
378 internal diameter of 6 m, which houses both the tracking and calorimetric system. This  
379 design allows for particles to be measured prior to crossing the magnetic coil which sig-  
380 nificantly improves the energy resolution.

381 **3.2.5 Muon Detector**

382 As implied by the detector's name, precise and robust muon measurements have been  
383 a central theme of the CMS experiment since the early stages of its design. The detector  
384 design takes into account that muons behave as minimum ionizing particles (MIPs) [15]  
385 and can therefore manage to traverse the tracker and calorimeters with minimal energy  
386 loss. Furthermore, due to their relatively long lifetime they can be efficiently identified  
387 by a dedicated system at the outer region of the detector. Consequently, the CMS muon  
388 systems comprise the outermost layer of the detector, which are integrated into the mag-  
389 net return yoke that surrounds the solenoid.

390

391 The muon system is capable of three main functions: muon identification, muon  $p_T$   
392 measurement and triggering. It is composed of three different types of detectors, all of  
393 which make use of gaseous chamber technology. This choice of detector provides a cost  
394 efficient way of covering most of the full solid angle, featuring a total of 25,000 m<sup>2</sup> of de-  
395 tection plates. As a consequence of the shape of the solenoid magnet, the muon detector  
396 was designed to have a cylindrical barrel section as well as two planar endcap regions.

397

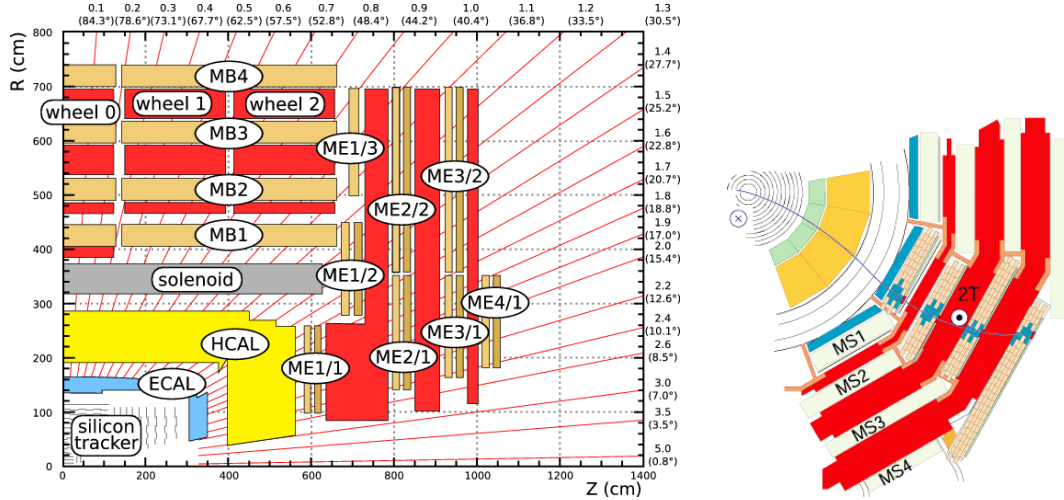


**Figure 3.7:** The left diagram shows a quarter-view of CMS with both the muon barrel (MB) and endcap (ME) stations [16]. The right diagram shows a muon in the transverse plane leaves a curved trajectory across the four muon detector stations [17].

398     For the barrel region of the muon detector, four layers of drift tube (DT) modules are  
 399    used, covering a pseudorapidity of up to  $|\eta| < 1.2$ . These four layers, called “stations”,  
 400    are arranged in cylindrical concentric layers around the beam line, where the first three  
 401    layers have 60 DTs each and the outer cylinder has 70. Each of the DT stations contain  
 402    12 individual gas filled tubes, all of which have a 4cm diameter and a center electrode.  
 403    The use of DTs as tracking detectors for the barrel muon system is possible because of  
 404    the low expected muon rate and the relatively low strength of the local magnetic field.

405

406     The endcap regions of the muon system are subject to a higher muon rate, and cover  
 407    the range  $0.9 < |\eta| < 2.4$  where the magnetic field is stronger and less homogeneous.  
 408    Considering these conditions, cathode strip chambers (CSCs) are employed, which fea-  
 409    ture high granularity, fast response time and adequate radiation hardness. CSCs consist of  
 410    arrays of positively-charged “anode” wires crossed with negatively-charged copper “cath-  
 411    ode” strips within a gas volume. They are trapezoidal in shape and can cover either  $10^\circ$   
 412    or  $20^\circ$  in  $\phi$ . Furthermore, CSCs have the advantage of featuring both precision muon  
 413    measurement and muon trigger in a single device.

414

415     The third type of detector used in the CMS muon system are called resistive plate  
 416    chambers (RPCs) and can be found in both the barrel and endcap regions. They consist

417 of gaseous parallel-plate detectors capable of providing precise timing information and  
418 adequate spatial resolution. Because of their excellent time resolution, RPCs provide the  
419 capability of tagging the time of an ionizing event between 2 consecutive LHC bunch  
420 crossings (BX) in a much shorter time ( $\sim 1$  ns) than the interval between the BXs (25  
421 ns). For this reason, an RPC-based dedicated muon trigger device can be implemented to  
422 unambiguously identify the relevant BX to which a muon track is associated with, despite  
423 the high rate of events and background expected at the LHC.

424 **3.2.6 Trigger and Data Acquisition**

425 Due to the vast volume of data originating from the proton-proton collisions (deliv-  
426 ered by the LHC at a rate of 40 MHz), a method of eliminating the majority of the un-  
427 interesting/unwanted events was a requisite for the CMS detector design. This event rate  
428 reduction is achieved by the implementation of the so-called trigger system, which man-  
429 ages to select the potentially interesting interactions and reduce the rate from a staggering  
430  $40 \text{ TBs}^{-1}$  to a manageable value of just a few hundred Hz.

431

432 The CMS trigger system is implemented using a two-stage rate reduction, which com-  
433 bines both a hardware and software phase. The combination of both of these triggers is  
434 designed to reduce the rate by a factor of  $\sim 10^6$ . The first stage used in the rate reduction  
435 is purely hardware based and it is called the Level 1 (L1) Trigger [18], which consists of  
436 both Field Programmable Gate Array (FPGA) and Application Specific Integrated Circuit  
437 (ASIC) technology. During this initial stage, the rate is reduced to about 100 kHz with  
438 a latency of  $3.2 \mu\text{s}$ . This time interval constrains the trigger decision, allowing only for  
439 data from the calorimeters and muon system to be processed. Trigger primitives (TP)  
440 from these subsystems are processed through a series of steps before the combined event  
441 information is evaluated by the global trigger (GT) where the final decision, whether or  
442 not to accept the event, is made.

443

**Figure 3.8:** Transverse slice of the CMS detector, showing the individual detector subsystems and particle signatures in each. The particle type can be inferred by combining the detector response in the different subdetectors [7].

444        The second stage, which implements offline-quality reconstruction algorithms in its  
 445     event selection, is referred to as the High-Level Trigger (HLT) [19]. The event selection  
 446     process for the HLT requires that physics objects for each event, such as electrons, muons  
 447     and jets, are reconstructed and undergo predetermined identification criteria.

### 448     3.2.7 Event Reconstruction

449        In order to reconstruct the events the particle flow (PF) algorithm [20] is used. This  
 450     algorithm gathers information from all the CMS sub-detectors to reconstruct charged and  
 451     neutral hadrons, photons, muons, and electrons. It relies on an efficient and pure track  
 452     reconstruction, a clustering algorithm able to distinguish overlapping tracks originated  
 453     from different vertices, and an efficient link procedure to associate each particle deposit  
 454     in the sub-detectors. Once all the deposits of a particle are associated, it can be correctly  
 455     identified and its four-momentum optimally determined from the combined information  
 456     of the sub-detectors. The resulting list of particles are then used to reconstruct higher level  
 457     objects such as jets, taus, missing transverse energy, and to compute charged lepton and  
 458     photon isolation, etc [21]. The CMS experiment is provided with millions of collisions  
 459     per second, which need to be triggered, detected, stored and analyzed in a collaboration of  
 460     several thousand physicists. This huge amount of data and the complexity of the detector  
 461     require a flexible data model that serves all the needs of the collaboration. The data for-  
 462     mat is optimized for performance and flexibility of the reconstruction for the end user's  
 463     analysis.

464

465        Event information from each step in the simulation and reconstruction chain is logi-  
 466     cally grouped into what is called a data tier [22]. From the physicist's point of view the  
 467     most important data tiers are RECO, which contains all reconstructed objects and hits,  
 468     and AOD (a subset of RECO). The AOD will contain a copy of all the high-level physics

469 objects (such as muons, electrons, taus, etc.) and enough information about the event to  
470 support all the typical usage patterns of a physics analysis. It also contains a summary of  
471 the RECO information sufficient to support typical analysis actions such as track refitting  
472 with improved alignment or kinematic constraints, re-evaluation of energy and/or posi-  
473 tion of ECAL clusters based on analysis-specific corrections. The format of each data tier  
474 is ROOT [23]. ROOT is a framework for data processing developed at CERN with the  
475 sole purpose of aiding high energy physics research. The various AOD datasets are stored  
476 worldwide at various data tier centers. From the AOD's the analysis groups create data  
477 structures called NTuples containing only the high-level physics objects needed for their  
478 particular analysis.

### 479 3.2.8 Future Upgrade of Pixel Detector

480 After the first LHC shutdown called LS1 (2013-2014), and the installation of the  
481 Phase-1 Pixel Detector [24] in early 2017, among other things, the LHC is planning an-  
482 other series of upgrades during two major shutdowns, called LS2 and LS3, currently  
483 planned for 2019-2020 and  $\sim$  2024, respectively. LS2 would result in a further increase  
484 of the luminosity beyond the original design value, to over  $2 \cdot 10^{34} \text{ cm}^{-2} \text{ s}^{-1}$ . With the  
485 LS3 upgrade of the LHC (called HL-LHC [25]) the luminosity is expected to reach up  
486 to  $7.5 \cdot 10^{34} \text{ cm}^{-2} \text{ s}^{-1}$ . Correspondingly, the CMS collaboration has planned a series of  
487 further upgrades [26, 27] that will ensure the capabilities of the CMS detector to match  
488 to the HL-LHC running conditions, while taking the opportunity to improve the perfor-  
489 mance and repair any problems uncovered during the data-taking periods. The UPRM  
490 group will continue its involvement in the Phase-1 Pixel Detector operations and Phase-2  
491 Pixel Upgrade design.

492

493 The HL-LHC conditions of instantaneous peak luminosities of up to  $7.5 \cdot 10^{34} \text{ cm}^{-2}$   
494  $\text{s}^{-1}$  and an integrated luminosity of the order of  $300 \text{ fb}^{-1}$  would result in 1 MeV neutron  
495 equivalent fluence of  $2.3 \cdot 10^{16} \text{ neq/cm}^2$  and a total ionizing dose (TID) of 12MGy (1.2

496 Grad) at the center of CMS, where its innermost component, the Phase-2 Pixel Detector  
497 will be installed. The detector should be able to withstand the above radiation dose, han-  
498 dle projected hit rates of  $3\text{GHz}/\text{cm}^2$  at the lowest radius, be able to separate and identify  
499 particles in extremely dense collision debris, deal with a pileup of 140-200 collisions per  
500 bunch crossing and have a high impact parameter resolution. This translates into requiring  
501 a detector design that is highly granular, has thinner sensors and smaller pixels, and faster,  
502 radiation hard electronics compared to its Phase-1 counterpart. The selection of interest-  
503 ing physics events at the Level-1 (L1) trigger and inefficiency of selection algorithms in  
504 high pileup conditions further require the Tracker to be included in this trigger stage, help-  
505 ing reduce the event rate from 40 MHz rate to 7.5 kHz. The physics goals also require  
506 an increase in Pixel Detector coverage to  $|\eta| = 4.0$  which improves the  $p_T^{miss}$  resolution  
507 and particle-flow event reconstruction by providing  $p_T$  measurements and trajectories for  
508 charged particles entering the calorimeters. The  $p_T^{miss}$  resolution is an essential perfor-  
509 mance parameter for many BSM physics searches including SUSY and extra dimension  
510 models where particles escape undetected from the detector space. The smaller pixel size  
511 will further improve b-tagging as well as hadronic reconstruction and track reconstruction  
512 efficiencies within boosted jets, which can be produced from new heavy objects decaying  
513 to Higgs, Z bosons, or top quarks – all heavy probes that can be exploited for new physics  
514 searches. Improving the b-tagging capabilities directly affects our analysis due to the im-  
515 portance of properly identifying top quark decays.

516

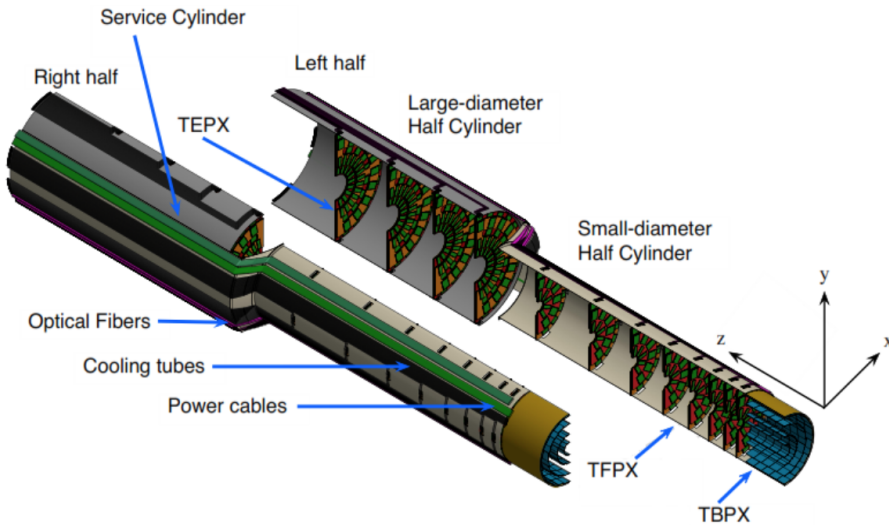


**Figure 3.9:** Phase-2 Pixel Detector Layout[ref].

517 The Phase-2 Pixel Detector [28, 29] baseline design comprises a barrel part with 4  
 518 layers of Tracker Barrel Pixel Detector (TBPX), 8 small double-discs per side of Tracker  
 519 Forward Pixel Detector (TFPX) and 4 large double-discs per side of Tracker Endcap Pixel  
 520 Detector (TEPX). This forward and end part is referred to as 8l4s (8 TFPX and 4 TEpx).  
 521 In the TBPX the pixel modules are arranged in “ladders”. In each layer, neighboring lad-  
 522 ders are mounted staggered in radius, so that  $r\text{-}\phi$  overlap between the ladders is achieved.  
 523 The modules on a ladder do not overlap in  $z$ . A projective gap at  $\eta = 0$  is avoided by  
 524 mounting an odd number of modules along  $z$ , and by splitting the barrel mechanics in  $z$   
 525 into slightly asymmetric halves. In TFPX and TEpx the modules are arranged in concen-  
 526 tric rings. Each double-disc is physically made of two discs, which facilitates to mount  
 527 modules onto four planes, with overlaps in  $r$  as well as  $r\text{-}\phi$ . Each disc is split into two  
 528 halves, and these D-shaped structures are referred to as “dees”. The TEpx will provide  
 529 the required luminosity measurement capability, by an appropriate implementation of the  
 530 readout architecture. In total, the pixel detector will have an active surface of approxi-  
 531 mately  $4.9 \text{ m}^2$ . [Figure 3.9](#) shows the layout of the Phase-2 Pixel Detector.

532 **Appendix A**

533 **Appendix Title**

534 **Appendix B**

535 **References**

- 536 [1] C. Lefevre, “The CERN accelerator complex. Complexe des accelerateurs du  
537 CERN.” Available on the [CERN document server](#), Dec 2008.
- 538 [2] T. Sakuma and T. McCauley, “Detector and Event Visualization with SketchUp  
539 at the CMS Experiment,” *J. Phys. Conf. Ser.*, vol. 513, p. 022032, 2014.  
540 [doi:10.1088/1742-6596/513/2/022032](https://doi.org/10.1088/1742-6596/513/2/022032).
- 541 [3] S. Spannagel, *CMS Pixel Detector Upgrade and Top Quark Pole Mass Determina-*  
542 *tion*, vol. 27. Springer, 2017. [doi:10.1007/978-3-319-58880-3](https://doi.org/10.1007/978-3-319-58880-3).
- 543 [4] CMS Collaboration, “CMS Physics Technical Design Report Volume 1: Detec-  
544 tor Performance and Software,” Technical Design Report CERN-LHCC-2006-001,  
545 CERN (2006).
- 546 [5] CMS Collaboration, “The CMS Experiment at the CERN LHC,” *JINST*, vol. 3,  
547 p. S08004, 2008. [doi:10.1088/1748-0221/3/08/S08004](https://doi.org/10.1088/1748-0221/3/08/S08004).
- 548 [6] CMS Collaboration, “Performance of the CMS Hadron Calorimeter with Cos-  
549 mic Ray Muons and LHC Beam Data,” *JINST*, vol. 5, p. T03012, 2010.  
550 [doi:10.1088/1748-0221/5/03/T03012](https://doi.org/10.1088/1748-0221/5/03/T03012).
- 551 [7] J. Nielsen, “Fundamentals of LHC Experiments,” in *Proceedings, Theoretical Ad-*  
552 *vanced Study Institute in Elementary Particle Physics (TASI 2010). String Theory*

- 553       *and Its Applications: From meV to the Planck Scale: Boulder, Colorado, USA, June*  
554       *1-25, 2010*, pp. 127–152, 2011. [arXiv:1106.2516](https://arxiv.org/abs/1106.2516).
- 555       [8] CMS, “The CMS Computing Project,” tech. rep., CERN, 2005.
- 556       [9] ATLAS Collaboration, “The ATLAS Experiment at the CERN Large Hadron Col-  
557       lider,” *JINST*, vol. 3, p. S08003, 2008. [doi:10.1088/1748-0221/3/08/S08003](https://doi.org/10.1088/1748-0221/3/08/S08003).
- 558       [10] LHCb Collaboration, “The LHCb Detector at the LHC,” *JINST*, vol. 3, p. S08005,  
559       2008. [doi:10.1088/1748-0221/3/08/S08005](https://doi.org/10.1088/1748-0221/3/08/S08005).
- 560       [11] K. Aamodt *et al.*, “The ALICE experiment at the CERN LHC,” *JINST*, vol. 3,  
561       p. S08002, 2008. [doi:10.1088/1748-0221/3/08/S08002](https://doi.org/10.1088/1748-0221/3/08/S08002).
- 562       [12] K. Garrett and G. Duda, “Dark Matter: A Primer,” *Adv. Astron.*, vol. 2011,  
563       p. 968283, 2011. [doi:10.1155/2011/968283](https://doi.org/10.1155/2011/968283).
- 564       [13] R. C. G. Landim, *Dark Sector Cosmology*. PhD thesis, Sao Paulo U., 2017.  
565       [arXiv:1702.06024](https://arxiv.org/abs/1702.06024).
- 566       [14] K. W. Bell *et al.*, “Vacuum phototriodes for the CMS electromagnetic  
567       calorimeter endcap,” *IEEE Trans. Nucl. Sci.*, vol. 51, pp. 2284–2287, 2004.  
568       [doi:10.1109/TNS.2004.836053](https://doi.org/10.1109/TNS.2004.836053).
- 569       [15] H. Bichsel, D. E. Groom, and S. R. Klein, “Passage of particles through matter,”  
570       2004.
- 571       [16] CMS Collaboration, “Alignment of the CMS Muon System with Cosmic-Ray  
572       and Beam-Halo Muons,” *JINST*, vol. 5, p. T03020, 2010. [doi:10.1088/1748-0221/5/03/T03020](https://doi.org/10.1088/1748-0221/5/03/T03020).
- 574       [17] “Muon Detectors.” <http://cms.web.cern.ch/news/muon-detectors>.  
575       Accessed: 2018-04-08.
- 576       [18] A. Tapper and D. Acosta, “CMS Technical Design Report for the Level-1 Trigger  
577       Upgrade,” 2013.

- 578 [19] W. Adam *et al.*, “The CMS high level trigger,” *Eur. Phys. J.*, vol. C46, pp. 605–667,  
579 2006. [doi:10.1140/epjc/s2006-02495-8](https://doi.org/10.1140/epjc/s2006-02495-8).
- 580 [20] F. Beaudette, *The CMS Particle Flow Algorithm*, 2013.
- 581 [21] A. K. Nayak, “Reconstruction of physics objects in the CMS detector,” *PoS*,  
582 vol. CHARGED2012, p. 010, 2012.
- 583 [22] CMS Collaboration, “CMS: The computing project. Technical design report,” Tech-  
584 nical Design Report CERN-LHCC-2005-023, CERN (2005).
- 585 [23] R. Brun and F. Rademakers, “ROOT: An object oriented data analysis frame-  
586 work,” *Nucl. Instrum. Meth.*, vol. A389, pp. 81–86, 1997. [doi:10.1016/S0168-9002\(97\)00048-X](https://doi.org/10.1016/S0168-9002(97)00048-X).
- 588 [24] M. Lipinski, “The Phase-1 upgrade of the CMS pixel detector,” *JINST*, vol. 12,  
589 no. 07, p. C07009, 2017. [doi:10.1088/1748-0221/12/07/C07009](https://doi.org/10.1088/1748-0221/12/07/C07009).
- 590 [25] G. Apollinari, I. Bejar Alonso, O. Bruning, M. Lamont, and L. Rossi, “High-  
591 Luminosity Large Hadron Collider (HL-LHC) : Preliminary Design Report,” 2015.  
592 [doi:10.5170/CERN-2015-005](https://doi.org/10.5170/CERN-2015-005).
- 593 [26] D. Contardo, M. Klute, J. Mans, L. Silvestris, and J. Butler, “Technical Proposal for  
594 the Phase-II Upgrade of the CMS Detector,” 2015. [CMS-TDR-15-02](https://cds.cern.ch/record/1900000).
- 595 [27] J. Pilot, “Future of the CMS Muon System: Upgrades and Aging,” *PoS*,  
596 vol. ICHEP2016, p. 281, 2016. [doi:10.22323/1.282.0281](https://doi.org/10.22323/1.282.0281).
- 597 [28] K. Klein, “The Phase-2 Upgrade of the CMS Tracker,” 2017. [CMS-TDR-014](https://cds.cern.ch/record/2200000).
- 598 [29] S. Mersi, “Phase-2 Upgrade of the CMS Tracker,” *Nucl. Part. Phys. Proc.*, vol. 273-  
599 275, pp. 1034–1041, 2016. [doi:10.1016/j.nuclphysbps.2015.09.162](https://doi.org/10.1016/j.nuclphysbps.2015.09.162).